

# Modification Mechanism of La-doped Ti/SnO<sub>2</sub> Electrodes from a micro-perspective: Electrochemical Analysis Compared with Theoretical Calculations

Qiang Bi<sup>1</sup>, Juanqin Xue<sup>1</sup>, Xiao Zhang<sup>1</sup>, Wenzhong Guan<sup>1</sup>, Yaowu Cui<sup>1</sup>, Le Ju<sup>2</sup>

<sup>1</sup> School of Metallurgy and Engineering, Xi'an University of Architecture and Technology, Xi'an 710055, China

<sup>2</sup> Xi'an GaoxinNo.1 High School, Xi'an 710056, China

\*E-mail: [bxqiang12@126.com](mailto:bxqiang12@126.com)

Received: 27 June 2017 / Accepted: 31 August 2017 / Published: 12 October 2017

---

Elemental doping can effectively improve the catalytic oxidation performance of titanium-based electrodes. To investigate the modification mechanism of La doping of Ti-based SnO<sub>2</sub> electrodes, the electrochemical behaviour of the electrodes was tested using anodic polarization curve, electrochemical impedance spectroscopy (EIS), linear sweep voltammetry (LSV), and the Mott-Schottky (M-S) techniques. The change in the SnO<sub>2</sub> internal lattice structure after La doping is the main reason for the improved performance. Therefore, theoretical calculations are used as an aid in the electrochemical analysis to study the underlying doping mechanism. The electronic structure and the density of SnO<sub>2</sub> lattice states in the electrode coating were calculated using first-principles calculations. Electrochemical tests and theoretical calculations are consistently shown that the doped La mainly improves the electrode performance through three aspects: 1) The band gap of the tin dioxide lattice was reduced, and the electrical conductivity of the electrode was improved; 2) The carrier of the tin dioxide lattice was increased, so that the electrode active site was increased; 3) The density of the tin dioxide lattice was changed, thereby changing the cyclic voltammetry and polarization characteristics of the electrode. The electrode performance is best as the La doping content gives the ratio Sn: Sb: La=100:10:1.5 and that the modification mechanism of the doping is revealed from a microscopic point of view.

---

**Keywords:** Modification mechanism; Electrochemical analysis; First-principles calculations; Ti/SnO<sub>2</sub> electrode

## 1. INTRODUCTION

In recent years, Ti-based tin dioxide electrodes for organic wastewater treatment have gained extensive attention due to their high oxygen evolution potential, fast reaction rate, and good

environmental compatibility [1-7]. Doping metal ions into oxides has been generally researched to promote the performance of electrodes. It was confirmed that doping can enhance the electro-catalytic activity and chemical or mechanical stability of oxide electrodes [8-10]. Rare earth elements, whose 4f and 5d electronic layer structures are not completely filled with electrons, are generally used as doping elements. Researchers prepared and inspected several tin dioxide electrodes doped with various rare earth elements, and the electrocatalytic performance of the electrodes were improved [11-13]. However, the doping modification mechanism is still obscure. Why the various kinds and quantities of doped metals directly affect the electrode performance is unknown. This study seeks to determine which properties of doped metal play the leading role in the electrode modification process and which microscopic properties of the electrode are changed by the metal doping.

The electrochemical behaviour of the electrode directly reflects the degradation efficiency of the pollutants. Studying the changes in the doping electrode electrochemical behaviour is an important way to explain the doping modification mechanism. However, most studies have focused on the CV and LSV analysis of the electrode [14-16], which only reflect the apparent performance of the electrode. EIS and M-S test data can better reflect the micro-electrode performance, such as the number of active sites and majority carrier [17,18], but previous research of these two aspects has been relatively limited.

In addition, determining the changes in the tin oxide electronic structure is the key to determining the underlying doping modification mechanism. First-principles calculations have been widely used as an outstanding tool to illustrate the electronic structure of crystalline materials [19-21]. Electronic and optical properties of SnO<sub>2</sub> powder were studied by first-principles calculations in several works [22-24]. Some investigators studied the electronic structure and stability of SnO<sub>2</sub> electrodes [25, 26], but few first-principles calculations regard the SnO<sub>2</sub> electrode electrocatalytic performance. The purpose of this work is to fill this research gap. Moreover, to highlight the role of La doping, simulations include La as the only element doped in the tin dioxide lattice without Sb.

In this work, we interpret the doping modification mechanism of a titanium-based, tin dioxide electrode through comprehensive electrochemical tests in combination with first-principles calculations.

## **2. EXPERIMENTAL**

### *2.1 Electrode preparation*

First, hydrochloric acid and ethylene glycol were mixed and agitated at 60°C until forming a homogeneous solution. Then, the solution was heated to 90°C followed by the addition of certain quantities of SnCl<sub>4</sub>·5H<sub>2</sub>O, Sb<sub>2</sub>O<sub>3</sub> and La<sub>2</sub>O<sub>3</sub>. After that, the solution was maintained at 90°C for 30 min to obtain a sol-gel. A 50 × 30 mm Ti substrate was polished by 180, 600 and 1000 mesh abrasive papers until the Ti substrate presented a metallic luster. After degreasing using a 10% sodium hydroxide solution, the Ti substrate was etched in boiling oxalic acid (10%, m/m) for 2 hours to produce a grey surface with a uniform roughness. The sol-gel solution was applied on the Ti substrate

by brushing, and then dried at 120°C. The above brushing and thermal treatment procedures were repeated 20 times, and the last calcination was annealed for 2 h at 500°C.

The proportions of Sn, Sb and La in the prepared electrode coating are 100:10:0, 100:10:1.0, 100:10:1.5, 100:10:2.0 and 100:10:2.5, respectively.

## 2.2 Electrochemical detection procedure

Electrochemical measurements were performed using a conventional three-electrode system installed in a PARSTAT-2273 electro-chemical workstation. The self-designed electrodes (10×10 mm) served as the work electrode, while a platinum sheet (10×10 mm) and a saturated calomel electrode were used as the counter and reference electrodes, respectively. The supporting electrolyte was 0.25 M Na<sub>2</sub>SO<sub>4</sub>. The anodic polarization curves were performed at a scan rate of 20 mV s<sup>-1</sup> over the potential range from 0 V to 2.5 V to determine the electroactivity of the electrodes in a 500 mg/L phenol solution. The EIS measurements were performed at a potential of 1.0 V (vs. SCE) over the frequency range from 100 kHz to 10 mHz with a signal amplitude of 5 mV in a 500 mg/L phenol solution. The LSV was performed at a sweep rate of 1.0 mV s<sup>-1</sup> over the potential range from 0 V to 2.5 V. The M-S characterization was performed at a fixed frequency of 1 kHz over the potential range from -0.4 V to 1.0 V. The latter two electrochemical tests were performed in a 1 M H<sub>2</sub>SO<sub>4</sub> solution.

The proportions of Sn, Sb and La in the electrode coating for electrochemical testing are 100:10:0, 100:10:1.0, 100:10:1.5, 100:10:2.0 and 100:10:2.5, respectively.

## 2.3 First-principles calculations

### 2.3.1 Calculation model

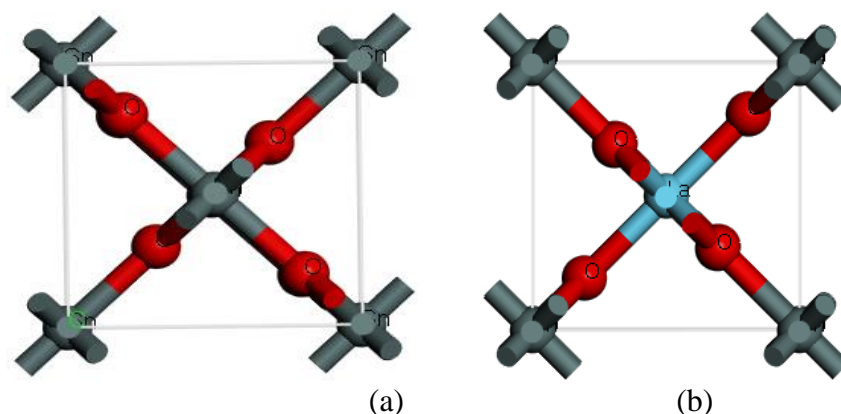


**Figure 1.** Scheme for the pure SnO<sub>2</sub> (a) and the La-doped SnO<sub>2</sub> (b) supercell structure.

The SnO<sub>2</sub> crystal is a rutile structure with a P<sub>42</sub>/mm space group. The lattice constants are a=b=0.4737 nm, and c=0.3186 nm, with α=β=γ=90° [27]. The lattice diagram for SnO<sub>2</sub> is shown in Fig. 1(a). In the crystal structure, Sn atoms are in the vertex and heart positions, O atoms form an octahedral structure around the Sn atoms and the proportion of Sn<sup>4+</sup> and O<sup>2-</sup> is 6:3. Fig. 1(b) shows the

unit cell of La-doped SnO<sub>2</sub> (La replace Sn). A La atom simply replaces a Sn atom, and the different concentrations of the La-doped SnO<sub>2</sub> crystal is established by changing the size of the super cell.

### 2.3.2 Calculation method

The first-principles calculations were performed using the Cambridge Serial Total Energy Package (CASTEP), which is a method of quantum mechanics using ab initio calculation based on DFT. The CASTEP uses the plane wave basis set for the expansion of the electronic wave functions. Electron-ion interactions are considered through the ultra-soft pseudo-potential and the force between the electrons can be corrected by the generalized gradient approximation (GGA) [28].

In the first-principles calculations process, the cut-off energy of the plane wave  $E_{\text{out}}$  is 380 eV, the energy of the structure convergence is  $5 \times 10^{-7}$  eV/atom in the self-consistent field (SCF), the energy convergence precision is  $5 \times 10^{-6}$  eV/atom in the iterative process, and The K values of the Brillouin Zone are sufficient. The force on each atom is not less than 0.01 V/Å and the stress is lower than 0.02 GPa. The calculated the energy is carried out in the reciprocal space. To obtain stable and accurate calculation results, the geometric structure of the ideal SnO<sub>2</sub> and La-doped SnO<sub>2</sub> unit cells were optimized before the calculation. Combined with the accurate unit cell parameters, the internal coordinates of the cell were subsequently optimized. In the whole calculation process, the electronic configurations of the three atomic species (La, Sn, O) are, respectively: [Xe]4f<sup>0</sup>5s<sup>2</sup>5p<sup>6</sup>5d<sup>1</sup>6s<sup>2</sup>, [Kr]5s<sup>2</sup>5p<sup>2</sup>, and [He]2s<sup>2</sup>2p<sup>4</sup>. The supercells and the La-doping ratios in a Sn<sub>1-x</sub>La<sub>x</sub>O<sub>2</sub> solid solution are shown in Tab. 1

**Table 1.** The supercells and the La-doping mole ratios.

	I	II	III	IV	V
Supercells	1×1×1	4×4×4	4×3×3	3×3×3	2×2×2
La-doping mole ratios	0%	0.78%	1.39%	1.85%	6.25%

## 3. RESULTS AND DISCUSSION

### 3.1 Electrochemical analysis

#### 3.1.1 Cyclic voltammetry

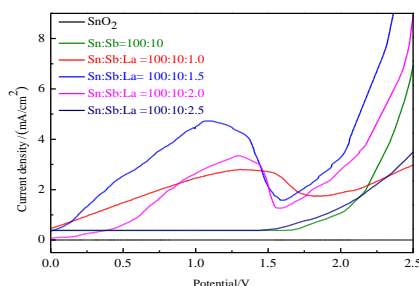


**Figure 2.** Anodic polarization curves of the La-doped Ti/Sb-SnO<sub>2</sub> electrode in a 500 mg/L phenol solution (scan rate: 20 mV s<sup>-1</sup> and potential range: 0 - 2.5 V).

In cyclic voltammetry detection, the peak current and the peak potential are the most important parameters. The anodic oxidation of the electrode is reflected in the voltage scan from negative to positive. The magnitude of the peak current and the peak potential in the anodic polarization curves can identify the direct electrooxidation activity of the electrode [29, 30].

The electrocatalytic activity of the electrode was studied using phenol as the target contaminant. Fig. 2 shows the anode anodic polarization curves obtained at the Ti/SnO<sub>2</sub>-Sb electrodes with different La doping levels in a 500 mg L<sup>-1</sup> phenol solution at a scan rate of 20 mV s<sup>-1</sup>. Fig. 2 shows clear phenol oxidation peaks from 0.75 to 1.5 volts. It was found that the intensity of the phenol oxidation peaks increased first and then decreased with the increase of the La doping level.

At a doping level of 0%, the phenol peak did not appear. With the increase of the doping level, the phenol peak began to increase and reached its maximum value as the doping level increased to Sn:Sb:La=100:10:1.5. As the amount of La doping continued to increase, the phenol peak began to decrease gradually and then disappeared at the doping level of Sn:Sb:La=100:10:2.5.

The larger oxidation peak current and the smaller oxidation peak potential indicate that the direct electrooxidation activity of phenol was stronger [31]. A larger peak current means that more electrons are transferred inside the electrode, which is, the electron transfer is easier after doping. This is consistent with the first principle calculation, as shown in Fig. 8, the band gap is the smallest when the concentration of La is 1.39%, which indicates that the valence band electrons require a minimum amount of energy to jump to the conduction band.

Considering the phenol oxidation peak, the Ti/La-SnO<sub>2</sub>-Sb electrode with a La doping level of 1.5% should be superior to electrodes with other phenol oxidation activities. La has a special 4f and 5d electron-layer structure, indicating that electron transfer is prone to occur. La doping into the SnO<sub>2</sub> lattice introduces a new impurity band, which provides a low energy level for the electron transfer, thus improving the conductivity of the SnO<sub>2</sub> electrode. In addition, the radius of the La<sup>3+</sup> ion is larger than the Sn<sup>4+</sup> ion, so the La doping led to a partial SnO<sub>2</sub> lattice expansion. This caused a charge imbalance and thus formed a new local energy level, which improved the electrocatalytic activity of the electrode. However, when the La doping content is increased, recombination of the electron-hole pairs is promoted, which decreased the electrocatalytic activity of the electrode [32].

### 3.1.2 Linear sweep voltammetry

The oxygen evolution reaction is the main side effect in the process of electrochemical oxidation on organic pollutants. The oxygen evolution potential (OEP) is an important parameter to evaluate the electrode electrooxidation capacity. A high OEP denotes a high degradation efficiency due to a low opportunity for the side reaction of oxygen formation [33]. The purpose of La doping is to increase the oxygen evolution potential of the electrodes. Fig. 3 shows the LSV curves of different electrodes. The OEP of the electrode increased first and then decreased with the increase of the La doping level. The maximum OEP level of the electrode is reached when the La doping ratio is 100:10:1.5.

The OEP is closely related to electrode coating composition and surface structure. As shown in Fig. 9, the results of the first principle calculation showed that the contribution of La atoms to the density of states varies with the doping concentration. This may be the reason of the different doped electrodes with different OEP.

In addition, La doping caused a rough, dense surface on these electrodes, which provided a large surface area with more active sites, which improved the oxygen evolution potential [34, 35]. The La-doped electrodes with higher OEP indicate their superior electrooxidation abilities and suitability for the organic pollutant degradation.

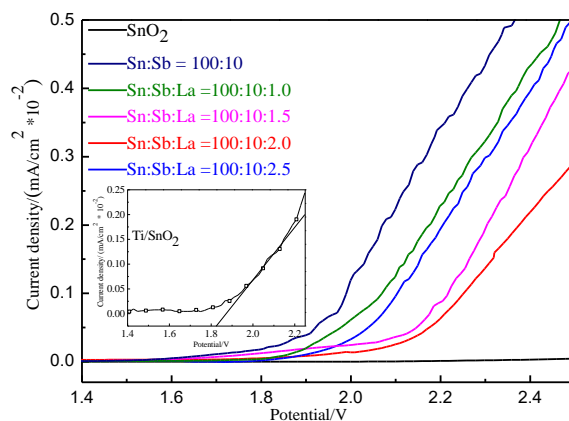


**Figure 3.** The LSV curves of the La-doped Ti/Sb-SnO<sub>2</sub> electrode in a 1.0 mol/L sulfuric acid solution (scan rate: 1.0 mV s<sup>-1</sup> and potential range: 0 V - 2.5 V).

### 3.1.3 Electrochemical impedance spectroscopy

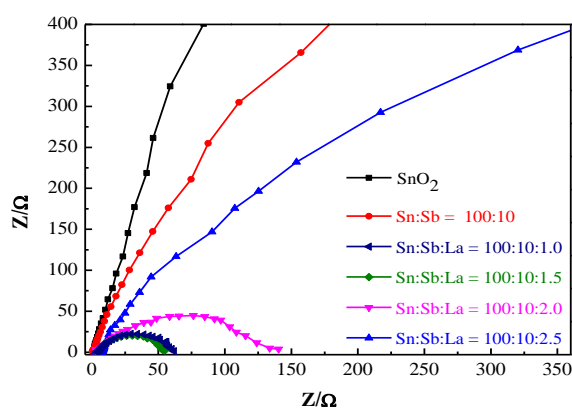


**Figure 4.** Nyquist plot of the La-doped Ti/Sb-SnO<sub>2</sub> electrode at 1.0 V potential in a 500 mg/L phenol solution (frequency range: 100 kHz-10 mHz and signal amplitude: 5 mV).

The EIS detection is applied to the electrode system with a small amplitude sine wave potential (or current) as the disturbance signal. The values of the equivalent circuit elements are obtained by the disturbance response of the electrode system to deduce the reaction mechanism of the electrode system. In the Nyquist plot of the impedance spectra, the semicircle portion at higher frequencies

corresponds to the charge-transfer limited process and at lower frequencies corresponds to the intermediate diffusion process [36]. Fig. 4 shows the EIS curves of different electrodes, and Fig. 5 shows the equivalent circuit of the electrochemical process.

In Fig. 5,  $R_s$ ,  $R_f$ , and  $R_{ct}$  represent the solution resistance, the membrane resistance between the coating/substrate and the Faraday transfer resistance, respectively. The  $C_f$  and  $C_{dl}$  are capacitive elements, which characterize the number of active sites on the electrode surface, where  $C_f$  represents the electric double layer capacitance of the coating and  $C_{dl}$  represents the electric double layer capacitance at the electrode/solution interface. The impedance spectra were fit using the equivalent circuit in Fig. 5, and the fitted values are shown in Tab. 2.

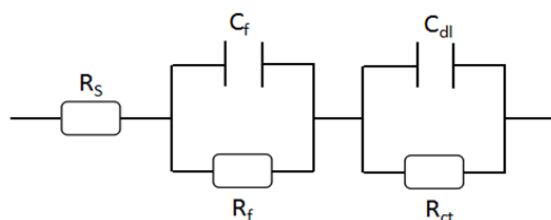


**Figure 5.** Equivalent circuit diagram of the electrochemical process.

As seen from Tab. 2, the solution resistance,  $R_s$ , is nearly constant. The membrane resistance,  $R_f$ , of the La-doped electrode is greater than that of the undoped electrode. This is because the number of hydroxyl radicals generated by the electrode changes with the different doping ratios and since the membrane resistance of the electrochemical reaction process is different. The reduction of the total resistance will be more conducive to the formation of  $\bullet\text{OH}$  [37], which is consistent with the semicircle trend from in Fig. 4. The  $C_{dl}$  of the electrode is proportional to the active charge of the electrode and, from Tab. 2, the electrode activity order can be determined:  $\text{Sn:Sb:La}= 100:10:1.5 > \text{Sn:Sb:La}=100:10:2.0 > \text{Sn:Sb:La}= 100:10:1.0 > \text{Sn:Sb}= 100:10 > \text{Sn:Sb:La}= 100:10:2.5 > \text{SnO}_2$ . The results show that the surface structure of the electrode was improved through doping, which resulted in more active charges on the surface of the electrode, and more  $\bullet\text{OH}$  radicals could be produced. The electrocatalytic activity was the highest when the La doping ratio is 100:10:1.5.

**Table 2.** The fitting values of the EIS curves for the La-doped Ti/Sb-SnO<sub>2</sub> electrode in a 500 mg/L phenol solution.

Electrode	$R_s$ ( $\Omega$ )	$C_f$ ( $\mu\text{F}$ )	$R_f$ ( $\Omega$ )	$C_{dl}$ ( $\mu\text{F}$ )	$R_{ct}$ ( $\Omega$ )
SnO <sub>2</sub>	0.21	0.22	2.13	14.1	4322
Sn: Sb=100:10	0.16	0.46	3.11	21.87	3009
Sn: Sb: La=100:10:1.0	0.35	59.2	49.3	173	75.2
Sn: Sb: La=100:10:1.5	0.54	112	4.69	322	52.9
Sn: Sb: La=100:10:2.0	0.15	3.07	14.97	236	131.4
Sn: Sb: La=100:10:2.5	0.33	2.87	8.72	11.32	772

The number of active sites on the electrode surface, has a direct relationship with the internal electron transfer and the number of carriers inside electrode, these are consistent with the calculation results of the Section 3.2.

### 3.1.4 Mott-Schottky characterization

As a semiconductor electrode, the flat band potential ( $E_{fb}$ ) reflects the position of the Fermi level [38], which has an important relationship with the electrocatalytic activity of the electrode. For n-type semiconductors, if  $E_{fb}$  becomes more negative, its catalytic activity becomes higher [39]. The increase of the donor density ( $N_D$ ) also implies an increase in the conductivity of the n-type semiconductor, which also contributes to improving the electrocatalytic activity of the semiconductor electrode.

When the metal oxide electrode is in contact with the solution, the semiconductor film and the solution are charged with opposite charges. The excess charge of the semiconductor film is distributed in the space charge layer. When the space charge layer is depleted, the space charge capacitance ( $C$ ) and potential ( $E$ ) can be expressed using the Mott-Schottky theory as Equation (1), and the flat band potential of the electrode is also determined.

$$\frac{1}{C^2} = \frac{-2}{\varepsilon\varepsilon_0eN_D S^2} \left( E - E_{fb} - \frac{KT}{e} \right) \quad (1)$$

where  $\varepsilon_0$  is the vacuum permittivity ( $8.85 \times 10^{-14}$  F/cm),  $\varepsilon$  is the dielectric constant of the tin dioxide film (taken as 14),  $N_D$  denotes the donor density,  $E_{fb}$  is the flat band potential,  $e$  is the electron charge ( $1.602 \times 10^{-19}$  C),  $T$  is the absolute temperature (298K),  $K$  is the Boltzmann constant and  $S$  is the surface area of the electrode.

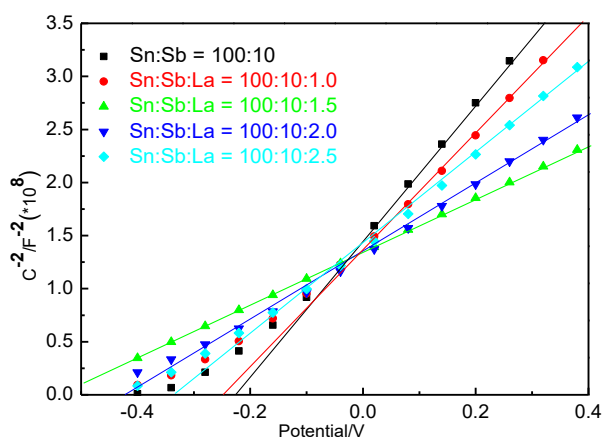


**Figure 6.** The Mott-Schottky curves of the La-doped Ti/Sb-SnO<sub>2</sub> electrode in a 1.0 mol/L sulfuric acid solution (fixed frequency: 1 kHz and potential range: -0.4 V-1.0 V).

Fig. 6 shows the Mott-Schottky curves for the different electrodes, and the fitted values of  $E_{fb}$  and  $N_D$  are shown in Tab. 3. It is readily observed that all the oxide coatings exhibit n-type semiconductor properties based on the slope of the curves [40]. As shown in Tab. 3, when the La

doping ratio is 100:10:1.5, the  $E_{fb}$  of the electrode is the most negative and the  $N_D$  is the largest. This means that the electrode has a high catalytic activity and good conductivity, which is consistent with the other electrochemical test results. And the electrochemical test results are consistent with first-principles calculations results, the calculated values of the density of states directly reflect the change of free carrier concentration.

**Table 3.** The fitting results of Mott-Schottky curves of the La-doped Ti/Sb-SnO<sub>2</sub> electrode.

Electrode	Sn:Sb= 100:10	Sn:Sb:La= 100:10:1.0	Sn:Sb:La= 100:10:1.5	Sn:Sb:La= 100:10:2.0	Sn:Sb:La= 100:10:2.5
$N_D (10^{38}) (cm^{-3})$	1.86	2.21	4.01	3.18	2.54
$E_{fb} (V)$	-0.30	-0.34	-0.54	-0.43	-0.37

The Mott-Schottky curves reflect some of the microscopic properties of the electrode, but more specific microscopic changes that are due to the doping can be calculated by first-principles calculations.

### 3.2 First-principles calculations

#### 3.2.1 Crystal structures and formation energies

After the geometric optimization, the lattice size, volume and formation of the SnO<sub>2</sub> and La-doped SnO<sub>2</sub> crystal were calculated, as shown in Tab. 4. The lattice sizes for the representative calculation of SnO<sub>2</sub> are  $a=b \approx 0.4737$  nm,  $c \approx 0.3187$  nm, which are approaching the experimental values and the values reported in the literature [41, 42]. This indicates that La doping does not change the configuration of the intrinsic SnO<sub>2</sub> crystal cell. Therefore, the crystal configuration and calculation results in this paper are reliable.

It can be seen from Tab. 4 that the volume of the unit cell gradually increased with the increase in the La doping ratio. This is because the La<sup>3+</sup> ion radius (0.106 nm) is larger than the Sn<sup>4+</sup> ion radius (0.071 nm). As the La is substituted for the Sn in the SnO<sub>2</sub> cell, the lattice volume is amplified. These results agree with quantum chemistry. Early experimental studies confirmed that appropriate doping can cause the grain growth to be relatively full and the crystal gap to decrease, which increased the surface adhesion of the SnO<sub>2</sub> and the electrode, while enhancing the electrocatalytic performance of the electrode [35]. The electrochemical test analysis in Section 3.1.1 on the charge balance changes and the energy level distribution caused by the electrode lattice expansion have also been verified through the calculations.

The formation energy of lattice is the key indicator to evaluate the stability of this configuration. As shown in Tab. 4, the formation energy of the La-doped SnO<sub>2</sub> decreases with the increase in the doping ratio. This indicates that proper doping does not affect the stability of the SnO<sub>2</sub> lattice, and that the doping modification technology is reliable.

**Table 4.** The optimized lattice parameters of the pure SnO<sub>2</sub> and La-doped SnO<sub>2</sub>.

	SnO <sub>2</sub>	Sn <sub>0.9922</sub> La <sub>0.0078</sub> O <sub>2</sub>	Sn <sub>0.9861</sub> La <sub>0.0139</sub> O <sub>2</sub>	Sn <sub>0.9815</sub> La <sub>0.0185</sub> O <sub>2</sub>	Sn <sub>0.9375</sub> La <sub>0.0625</sub> O <sub>2</sub>
Lattice Parameters (nm)	a=b=0.47372 c=0.31864	a=b=0.47373 c=0.31864	a=b=0.47375 c=0.31866	a=b=0.47375 c=0.31871	a=b=0.47381 c=0.31889
Volume (nm <sup>3</sup> )	0.0715	0.0715	0.0718	0.0719	0.0726
Formation Energies (eV)	-5.38	-5.59	-5.66	-5.74	-6.06

### 3.2.2 Band structures

To compare the electrocatalytic performance of the doped electrode, the band structures of the doped and undoped SnO<sub>2</sub> lattices were calculated and compared, and the results are shown in Fig. 7. Compared with the intrinsic SnO<sub>2</sub>, the band structure of the doped SnO<sub>2</sub> is degenerate, and the bottom of the conduction band and the top of the valence band of the doped system are located in the same point of the Brillouin zone, which shows the La-doped SnO<sub>2</sub> is a direct band gap semiconductor.

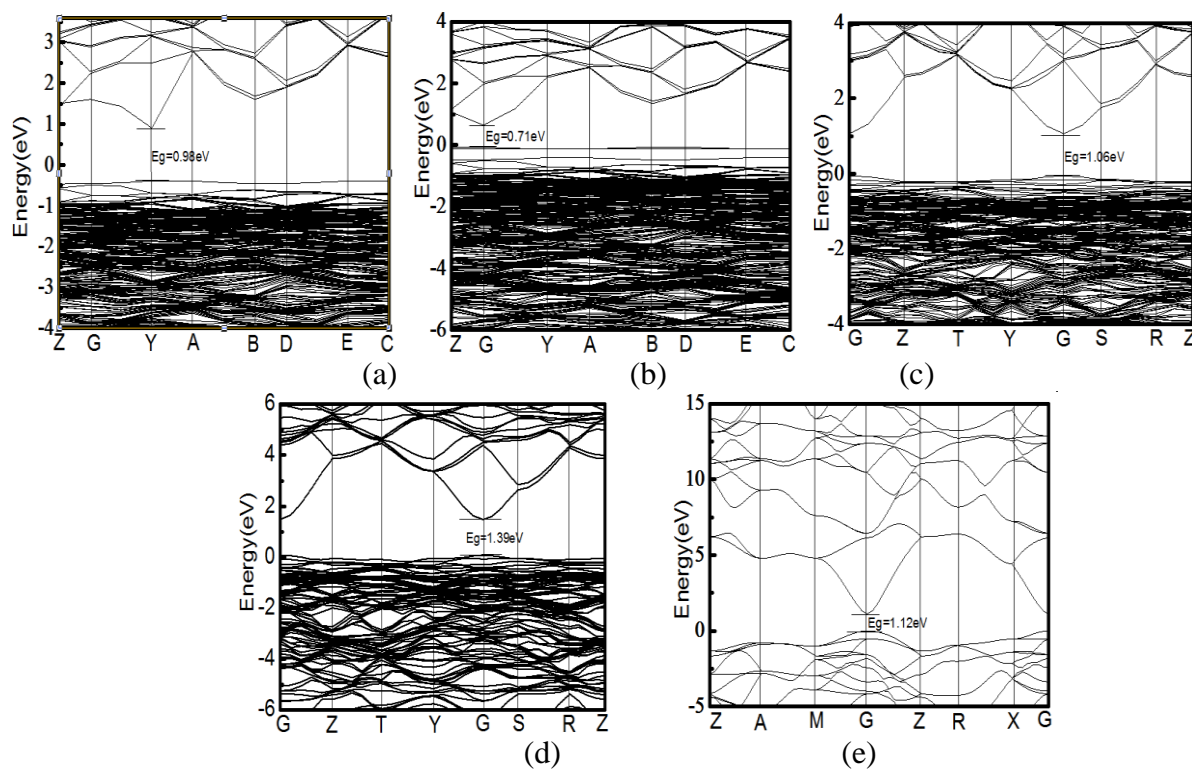


**Figure 7.** The energy band structure of different lattices (a: Sn<sub>0.9922</sub>La<sub>0.0078</sub>O<sub>2</sub>, b: Sn<sub>0.9861</sub>La<sub>0.0139</sub>O<sub>2</sub>, c: Sn<sub>0.9815</sub>La<sub>0.0185</sub>O<sub>2</sub>, d: Sn<sub>0.9375</sub>La<sub>0.0625</sub>O<sub>2</sub>, and e: SnO<sub>2</sub>).

Fig. 7 shows that the band gap of the doped SnO<sub>2</sub> first decreased and then increased with the increase of the La doping ratio, with the results summarized in Fig. 8. It is apparent that the band gap is the smallest when the concentration of La is 1.39%, which indicates that the valence band electrons require a minimum amount of energy to jump to the conduction band. Therefore, the conductivity of the electrode was improved by doping. At the same time, La<sup>3+</sup> replaced Sn<sup>4+</sup>, resulting in a partial lattice expansion and charge imbalance, which formed vacancy defects in the semiconductor material. With the increase of the La doping concentration, the content of oxygen vacancies in the SnO<sub>2</sub> crystal increased, causing the carrier concentration to increase. This increased the redox ability of the SnO<sub>2</sub>, and thereby, the electrocatalytic performance of the SnO<sub>2</sub> electrode was greatly improved.

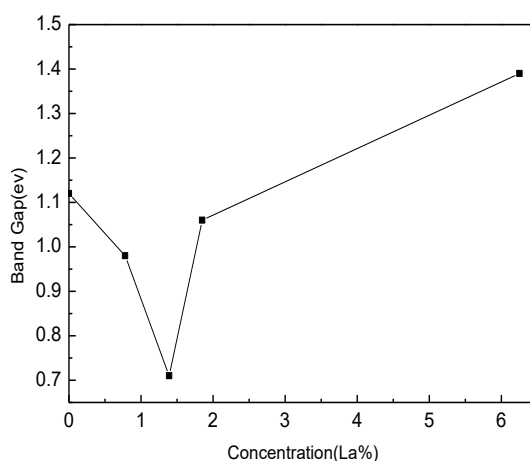


**Figure 8.** The change in the band gap of the La-doped SnO<sub>2</sub> with the concentration ratio.

However, a doping level that is too high will damage the SnO<sub>2</sub> lattice structure, and the energy level of the impurities can be extended to the impurity band. Instead, this will increase the band gap, and reduce the electrical conductivity and the electrocatalytic performance of the SnO<sub>2</sub> electrode. The calculated results agree with the electrochemical tests and the experimental results of the previous wastewater treatment process [43, 44]. Therefore, the SnO<sub>2</sub> electrode performance is the best when the La doping ratio is Sn:Sb:La= 100:10:1.5.

### 3.2.3. Density of states

To further analyse the contribution of the La doping to improve the conductivity and catalytic activity of the electrode, the density of the doped and undoped SnO<sub>2</sub> lattice states were calculated, as shown in Fig. 9. It can be seen from Fig. 9 that the density of La-doped SnO<sub>2</sub> states first increased and then decreased but are all significantly higher than that of the intrinsic SnO<sub>2</sub> lattice. This shows that the doped SnO<sub>2</sub> had more electrons involved in the electron transfer process, which significantly increased the free carrier concentration. Compared with the undoped SnO<sub>2</sub>, the free carriers in the doped lattice are mainly provided by the La 6s, La 5p and La 5d orbitals.

According to other literature analyses on the doping process [45, 46], in the conduction band bottom region (0~6 eV), the free carriers were mainly provided by the substitution of the La 5p and La 6s for the Sn 5s and Sn 5p. In the valence band top (-5~0 eV), the free carriers are mainly provided by the substitution of Sn 5s, O 2p, La 5d and La 5p for the Sn 5p and O 2p. With the increase in the La doping concentration, the number of electrons first increases and then decreases. As a result, more electrons can move between the valence band and the conduction band, which changed the electrical conductivity and catalytic properties of the electrode.

The contribution of La atoms to the density of states varies with the doping concentration. The contribution of the La atoms to the density of states is the largest at a 1.39% doping concentration. So far, the fundamental doping modification mechanism of the La-doped SnO<sub>2</sub> electrode had been explored from the atomic level.

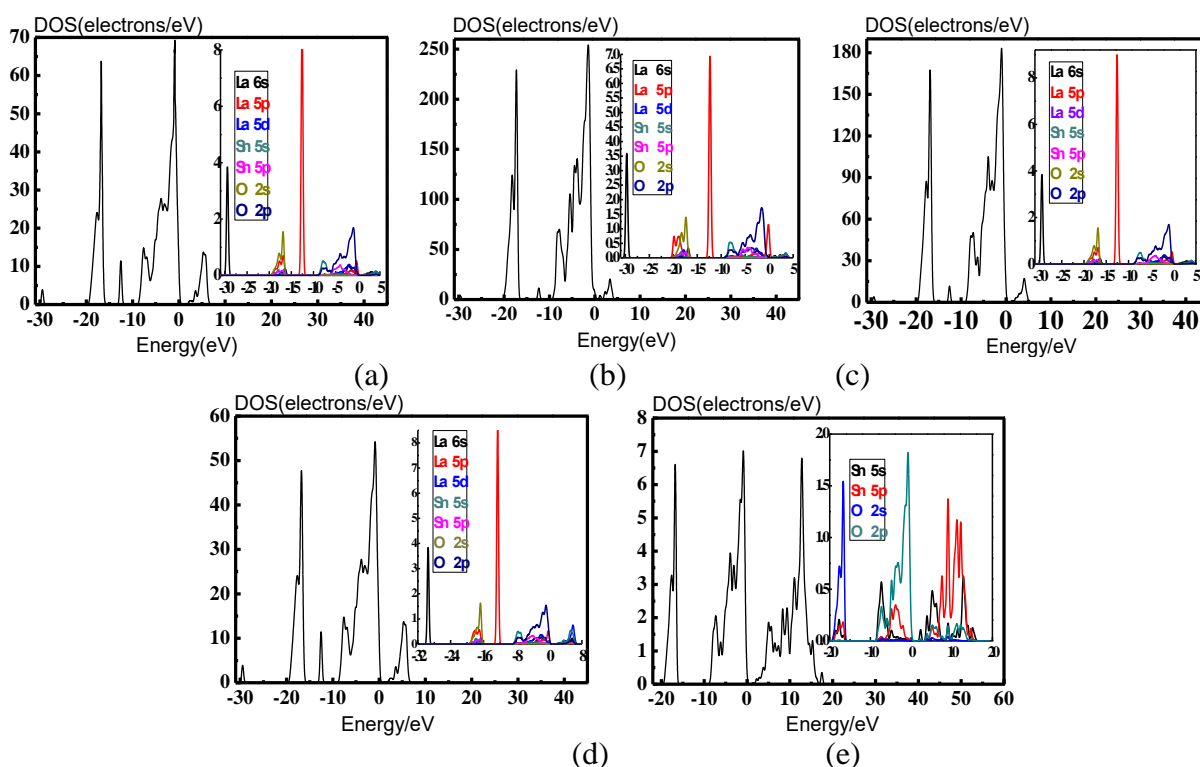


**Figure 9.** The density of states for different lattices (a: Sn<sub>0.9922</sub>La<sub>0.0078</sub>O<sub>2</sub>, b: Sn<sub>0.9861</sub>La<sub>0.0139</sub>O<sub>2</sub>, c: Sn<sub>0.9815</sub>La<sub>0.0185</sub>O<sub>2</sub>, d: Sn<sub>0.9375</sub>La<sub>0.0625</sub>O<sub>2</sub>, and e: SnO<sub>2</sub>).

#### 4. CONCLUSIONS

The experimental results show that doping with rare-earth element La can effectively improve the electrocatalytic activity of SnO<sub>2</sub> electrodes. Electrochemical tests show that the doping did not change the majority carrier of the SnO<sub>2</sub> n-type semiconductor. The CV, LSV, EIS and M-S test results are all self-consistent: the doped electrode revealed a good conductivity and electrocatalytic activity. When the La doping ratio is Sn:Sb:La= 100:10:1.5, the oxygen evolution potential of the electrode is the highest and the side reaction of the electrochemical process is the least, allowing more favourable

oxidation-reduction reactions to occur. Moreover, at the doping ratio of Sn:Sb:La= 100:10:1.5, the electrode possesses a more negative flat band potential, more carriers and more active sites. La doping caused microscopic changes in the SnO<sub>2</sub> electrode, which improved its overall performance.

To further reveal the mechanism of the doping modification, the electronic structure and the density of states of the doped and intrinsic SnO<sub>2</sub> lattice were compared using first-principles calculations. The fundamental reasons for the excellent performance of the electrodes were discussed at the molecular level. Due to the doping of La, the electrons in the La 5p and 6s orbitals provided more carriers between the conduction band and the valence band to improve the conductivity and electrocatalytic activity of the electrode. Moreover, the result showed that the combination of electrochemical analysis and quantum computing is an effective means to study the doping modification mechanism.

#### ACKNOWLEDGEMENTS

The authors gratefully acknowledge the financial support from the National Natural Science Foundation of China (51278407, 51408468, 51478379), and the scientific research project of Shaanxi Provincial Education Department (14JK1434).

#### References

1. F. T. Chen, S. C. Yu, X. P. Dong, S. S. Zhang, *J. Hazard. Mater.*, 227- 228 (2012) 474-479.
2. W. Ma, Z. H. Cheng, Z. X. Gao, R. Wang, B. D. Wang, Q. Sun, *Chem. Eng. J.*, 241 (2014) 167-174.
3. F. Sopaj, M. A. Rodrigo, N. Oturan, F. I. Podvorica, J. Pinson, M. A. Oturan, *Chem. Eng. J.*, 262 (2015) 286-294.
4. F. C. Moreira, J. Soler, A. Fonseca, I. Saraiva, R. A. R. Boaventura, E. Brillas, V. J. P. Vilar, *Water Res.*, 81(2015) 375-387.
5. M. A. M. Cartaxo, C. M. Borges, M. I. S. Pereira, M. H. Mendonça, *Electrochim. Acta*, 176 (2015) 1010-1018.
6. J. H.Q. Lee, B. K. Tay, R. Ganguly, R. D. Webster, *Electrochim. Acta*, 184 (2015) 392-402.
7. J. Kocábová, J. Fiedler, I. Degano, R. Sokolová, *Electrochim. Acta*, 187 (2016) 358-363.
8. Q. Z. Dai, J. Z. Zhou, X. Y. Meng, D. L. Feng, C. Q. Wu, J. M. Chen, *Chem. Eng. J.*, 289 (2016) 239-246.
9. M. Shestakova, M. Vinatoru, T. J. Mason, M. Sillanpaa, *Ultrason. Sonochem.*, 23 (2015) 135-141.
10. R. A. Herrada, A. Medel, F. Manríquez, I. Sirés, E. Bustos, *J. Hazard. Mater.*, 319 (2016) 102-110.
11. Y. H. Cu, Y. J. Feng, Z. Q. Liu, *Electrochim. Acta*, 54 (2009) 4903-4909.
12. M. H. M. T. Assumpcao, A. Moraes, R. F. B. De Souza, I. Gaubeur, R. T. S. Oliveira, V. S. Antonin, G. R. P. Malpass, R. S. Rocha, M. L. Calegaro, M. R. V. Lanza, M. C. Santos, *Appl. Catal. A*, 411- 412 (2012) 1- 6.
13. F. Deganello, L. F. Liotta, S. G. Leonardi, G. Neri, *Electrochim. Acta*, 190 (2016) 939-947.
14. S. A. M. Refaey, F. Taha, T. H. A. Hasanin, *Appl. Surf. Sci.*, 227 (2004) 416-428.
15. H. M. Villullas, F. I. Mattos-Costa, P. A. P. Nascente, L. O. S. Bulhões, *Electrochim. Acta*, 49 (2004) 3909-3916.
16. P. D. Yao, *Desalination*, 267 (2011) 170-174.
17. W. H. Yang, W.T. Yang, X. Y. Lin, *Appl. Surf. Sci.*, 258 (2012) 5716-5722.
18. D. Devilliers, E. Mahé, *Electrochim. Acta*, 55 (2010) 8207-8214.
19. Y. H. Fang, G. F. Wei, Z. P. Liu, *Catal. Today*, 202 (2013) 98-104.

20. N. G. Hormann, M. Jackle, F. Gossenberger, T. Roman, K. Forster-Tonigold, M. Naderian, S. Sakong, A. Groß, *J. Power Sources*, 275 (2015) 531-538.
21. R. Jinnouchi, T. Hatanaka, Y. Morimoto, M. Osawa, *Electrochim. Acta*, 101 (2013) 254-261.
22. H. Yahla, A. Boukra, M. Belhakem, P. E. Lippens, *Solid State Commun.*, 149 (2009) 2202-2206.
23. Q. J. Liu, Z. T. Liu, L. P. Feng, *Mater. Sci.*, 47 (2010) 1016-1022.
24. W. Zhou, L. J. Liu, M. Y. Yuan, Q. G. Song, P. Wu, *Mater. Sci.*, 54 (2012) 109-114.
25. Z. H. Liang, Y. B. Ding, J. Q. Jia, C. M. Fan, P. D. Han, *Physica B*, 406 (2011) 2266-2269.
26. X. J. Xie, J. Q. Jia, L. J. Han, X. L. Song, L. P. Zhong, Z. H. Liang, C. M. Fan, P. D. Han, *Physica B*, 421 (2013) 132-137.
27. A. A. Bolzan, C. Fong, B. J. Kennedy, C. J. Howard, *Acta Cryst. B*, 53(1997) 373-380.
28. J. Q. Jia, W. T. Zhang, Z. H. Liang, X. C. Zhang, C. C. Fan, P. D. Han, *Physica B*, 407 (2012) 1985-1989.
29. L. Z. Wang, S. X. Yang, B. Wu, P. Li, Z. N. Li, Y. M. Zhao, *Electrochim. Acta*, 206 (2016) 270-277.
30. P. Kucerová, J. Skopalová, L. Kucera, J. Táborický, H. Švecová, K. Lemr, P. Cankar, P. Barták, *Electrochim. Acta*, 215 (2016) 617-625.
31. C. Ramírez, M. A. del Valle, M. Isaacs, F. Armijo, *Electrochim. Acta*, 199 (2016) 227-233.
32. D. He, S. Mho, *J. Electroanal. Chem.*, 568 (2004) 19-27.
33. Y. Duan, Y. Chen, Q. Wen, T. G. Duan, *J. Electroanal. Chem.*, 768 (2016) 81-88.
34. Y. H. Cui, Y. J. Feng, Z. Q. Liu, *Electrochim. Acta*, 54 (2009) 4903-4909.
35. Q. Bi, J. Q. Xue, C. Tang, L. H. Yu, G. P. Li, X. Zhang, *Int. J. Electrochem. Sci.*, 11 (2016) 7412-7429.
36. K. Arora, N. Prabhakar, S. Chand, B. D. Malhotra, *Biosens. Bioelectron.*, 23 (2007) 613-620.
37. M. Muti, A. Erdem, A. Caliskan, A. Sinag, T. Yumak, *Colloids Surf. B*, 86 (2011) 154-157.
38. L. Lin, J. M. Lin, J. H. Wu, S. C. Hao, Z. Lan, *Mater. Res. Innovations*, 14 (2010) 370-374.
39. F. Ye, J. L. Li, X. D. Wang, T. T. Wang, S. M. Li, H. J. Wei, Q. F. Li, E. Christensen, *Int. J. Hydrogen. Energ.*, 35 (2010) 8049-8055.
40. H. H. Ge, X. M. Xu, L. Zhao, F. Song, J. Shen, G. D. Zhou, *J. Appl. Electrochem.*, 41 (2011) 519-525.
41. W. H. Yang, W. C. Lu, X. Y. Xue, Q. J. Zang, *Comput. Theor. Chem.*, 1069 (2015) 119-124.
42. Z. H. Deng, J. F. Yan, F. C. Zhang, X. W. Wang, J. P. Xu, Z. Y. Zhang, *Acta Photonica Sinica*, 36 (2007) 110-115.
43. Q. Bi, J. Q. Xue, L. H. Yu, C. Wang, F. L. Yu, *J. Chin. Rare Earth Soc.*, 31 (2013) 465-472.
44. Q. Bi, J. Q. Xue, L. H. Yu, C. Wang, F. L. Yu, J. Zhang, *Chem. Ind. Eng. Prog.*, 32 (2013) 3015-3020.
45. M. Nakayama, R. Jalem, T. Kasuga, *Solid State Ionics*, 262 (2014) 74-76.
46. M. M. Guo, X. J. Xie, J. Q. Jia, Z. H. Liang, C. M. Fan, P. D. Han, *Electrochim. Acta*, 151 (2015) 177-185.